

Fast-Ion Dynamics in the TEXTOR Tokamak Measured by Collective Thomson Scattering

H. Bindslev,^{1,*} S. K. Nielsen,¹ L. Porte,⁵ J. A. Hoekzema,² S. B. Korsholm,^{1,3} F. Meo,¹ P. K. Michelsen,¹ S. Michelsen,¹ J. W. Oosterbeek,² E. L. Tsakadze,¹ E. Westerhof,⁴ P. Woskov,³ and the TEXTOR team

¹EURATOM-Risø National Laboratory, DK-4000 Roskilde, Denmark

²EURATOM-Forschungszentrum Jülich GmbH, Institut für Plasmaphysik, D-52425 Jülich, Germany

³MIT Plasma Science and Fusion Center, Cambridge, Massachusetts 02139, USA

⁴FOM-Institute for Plasma Physics Rijnhuizen, EURATOM-FOM, The Netherlands

⁵CRPP, EURATOM-Confédération Suisse, EPFL, CH-1015 Lausanne, Switzerland

(Received 13 September 2006; published 16 November 2006)

Here we present the first measurements by collective Thomson scattering of the evolution of fast-ion populations in a magnetically confined fusion plasma. 150 kW and 110 GHz radiation from a gyrotron were scattered in the TEXTOR tokamak plasma with energetic ions generated by neutral beam injection and ion cyclotron resonance heating. The temporal behavior of the spatially resolved fast-ion velocity distribution is inferred from the received scattered radiation. The fast-ion dynamics at sawteeth and the slowdown after switch off of auxiliary heating is resolved in time. The latter is shown to be in close agreement with modeling results.

DOI: [10.1103/PhysRevLett.97.205005](https://doi.org/10.1103/PhysRevLett.97.205005)

PACS numbers: 52.25.Os, 52.40.Db, 52.50.Gj, 52.70.Gw

Fast-ion populations play an increasingly important role in the dynamics of magnetically confined plasmas as the conditions for a fusion power plant are approached [1–3]. Approximately one-third of the plasma energy is generally in the fast-ion populations. This energy must be channeled into heating the bulk plasma but can also drive waves, which affect confinement of bulk plasma and fast ions. Fast ions can, for instance, be prematurely ejected by Alfvén modes driven by the fast ions [4–8], and sawteeth are affected by fast ions and may redistribute fast ions [9–13].

Understanding the dynamics of fast ions and their interaction with the bulk plasma requires measurements of the confined fast-ion populations resolved in time, space, and velocity. This is expressed in the ITER diagnostic requirements [14,15]. Collective Thomson scattering (CTS) has the potential to provide such measurements [16] and to meet the ITER diagnostic requirements [17,18] and resolve the fusion alphas against a background neutral beam injection (NBI) fast-ion population [19]. CTS is based on the scattering of electromagnetic waves off microscopic fluctuations driven by ion motion [20–24]. The first CTS measurements of ion temperature in magnetically confined plasmas were done using far infrared radiation [25]. With gyrotrons as the source of probing radiation [26], the ion temperature was since measured with millimeter waves [27,28]. The first CTS measurement of a fast-ion velocity distribution was done at the Joint European Torus [16]. Other CTS experiments [29–31], though not yielding ion data, contributed by widening the experience with operating CTS diagnostics.

The breakthrough with routine CTS measurements of fast-ion populations in a magnetically confined plasma, resolving ≈ 100 time slices at intervals of 4 ms in each plasma shot, was achieved with the millimeter-wave CTS at TEXTOR. Some of these results are reported here.

The probing radiation for the TEXTOR CTS is provided by a 110 GHz gyrotron operated at 150 kW. With a central toroidal field of 2.6 T, the CTS spectra are at a local minimum in the electron cyclotron emission (ECE) spectrum between the fundamental and second harmonic ECE features. The probing radiation is launched from the low field side in the equatorial plane, and the receiver antenna is located ≈ 20 cm above the entry of the probing beam. Both transmitter and receiver have steerable, near Gaussian beam, antenna patterns. Measurements are spatially localized to the *scattering volume* where the probe and receiver beams overlap. They resolve the microscopic fluctuations with wave vector $\mathbf{k}^\delta = \mathbf{k}^s - \mathbf{k}^i$ and provide information on the distribution of ion velocities in the direction of \mathbf{k}^δ . Here \mathbf{k}^s and \mathbf{k}^i are the wave vectors of, respectively, the received scattered radiation and the probe, both in the scattering volume. Varying the antenna orientations, the location of the scattering volume can be shifted across most of the plasma cross section, and the resolved velocity direction can be varied from near parallel to near perpendicular to the magnetic field. Depending on scattering geometry, the radial resolution is 5–10 cm as evidenced by the spectral CTS data presented in Fig. 1, where the toroidal angle of the receiver antenna was scanned during a plasma shot. These data are also good evidence that the signals are indeed the result of scattering from the probe beam in the plasma. The received scattered radiation is detected using a heterodyne receiver with 32 (upgraded to 42) spectral channels with bandwidths from 80 to 750 MHz, giving complete coverage from 107 to 113 GHz. Notch filters are used to reduce stray radiation. Further details on the diagnostic and its upgrades can be found in Refs. [32–36].

To distinguish the fast-ion CTS signal with spectral power density around 1–10 eV from the ECE background of typically 10–100 eV, the gyrotron is modulated with a

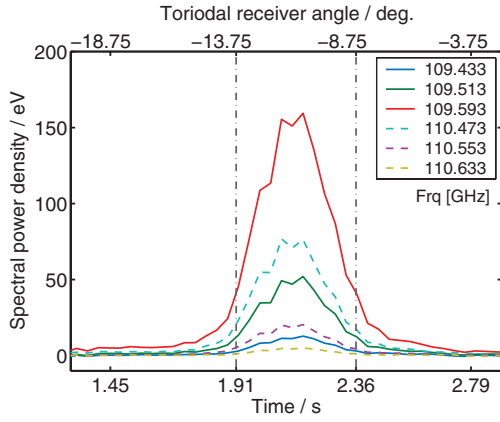


FIG. 1 (color). CTS spectral data recorded for an Ohmic plasma where the toroidal angle ϕ_r of the receiver viewing direction was scanned during the plasma shot. The plot shows CTS spectral power density in a number of channels vs time and ϕ_r . Receiver and probe beams go through overlap for a variation of 5° of ϕ_r . With a distance from receiver antenna to scattering volume of 50 cm, this corresponds to a width of the scattering volume of 4 cm in the direction perpendicular to the probe and receiver beam directions. In the direction of \mathbf{k}^δ , the extent of the scattering volume is $\approx 5/2$ times larger. Shot number 100467. $\angle(\mathbf{k}^\delta, \mathbf{B}) = 110^\circ$. Scattering volume at $R = 1.8$ m, $z = 0$ m.

period of 4 ms and a 50% duty cycle, giving a time resolution of 4 ms. This is illustrated in Fig. 2, where the spectral power density in the channel centered at 110.9 GHz is plotted versus time for shot 89510. The samples recorded when the gyrotron was off (on) are shown as blue (red) and are thus due to ECE (ECE + CTS). The background noise to our measurement is actually ECE and detector noise. For simplicity, we refer to the sum as ECE. ECE signals are recorded when the gyrotron is off and continuously monitored in channels several gigahertz away from the gyrotron frequency where no scattered radiation is observed nor expected. From these signals, the ECE during gyrotron pulses can be estimated for each channel. The green line in Fig. 2 shows such an ECE estimate. The CTS signal is estimated by subtracting the ECE estimate from the signals recorded when the gyrotron is firing.

The ECE is strongly perturbed by sawteeth at 2.03, 2.12, and 2.23 seconds. It is noteworthy that despite this the estimated CTS signal at 110.9 GHz has no visible signature of sawteeth as seen in Fig. 3, where the CTS time trace for 110.9 GHz is plotted together with CTS signals at four other frequencies for shot 89510. In the channels covering the frequencies from 100.58 to 100.74 GHz, clear signatures of sawteeth are present, which, on account of the robustness of the ECE subtraction, we ascribe entirely to sawtooth related variations in the CTS spectral power density.

In Fig. 4, the CTS spectral power density for shot 89510 is plotted as a function of time and frequency over the full CTS bandwidth with data from 21 channels from which

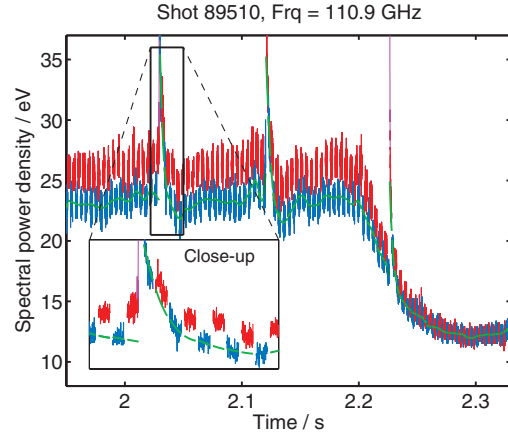


FIG. 2 (color). Raw data time trace for a CTS channel. Blue indicates ECE background and red refers to gyrotron on time (CTS + background). The green line represents the reconstructed background during the gyrotron probing time.

data were recorded. No data are shown for frequencies near the probe frequency where the notch filter blocks signals.

From the CTS spectral power density, the fast-ion 1D velocity distribution is inferred [37] on the basis of a fully electromagnetic CTS model [23]. The inferred distribution is shown in various forms in Figs. 5, 6, and 8(a).

In TEXTOR shot 89510, the fast ions were generated by ~ 1.3 MW neutral beam injection of ~ 50 keV deuterons in the cocurrent direction and by ~ 1.0 MW minority ion cyclotron resonance heating (ICRH) of hydrogen with a frequency of 38 MHz giving rise to a resonance layer slightly on the low field side of the vessel center. The orientations of the probe and receiver beams were such that the resolved fluctuation wave vector \mathbf{k}^δ , and, hence, the direction in which the velocity was resolved, made an angle to the static magnetic field of 113° . The scattering volume was at $R = 1.61 \pm 0.08$ m and $z = 0 \pm 0.03$ m. These values were estimated by ray tracing. The scattering volume was located on the high field side of the plasma

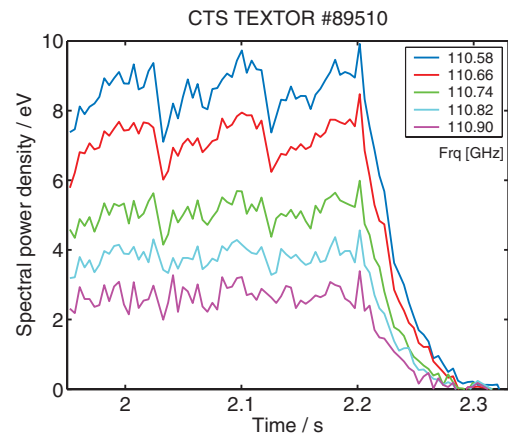


FIG. 3 (color). CTS spectral power densities in five channels vs time trace. The channels are labeled by their center frequencies. Shot number 89510.

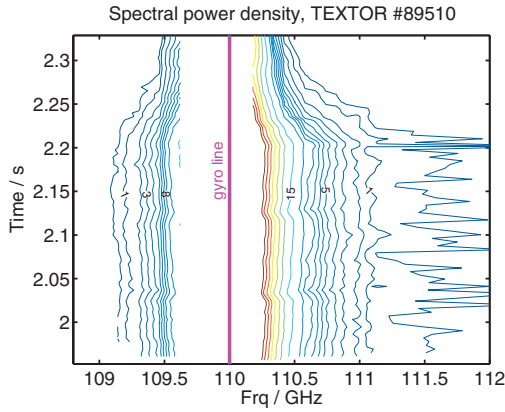


FIG. 4 (color). CTS spectral power density as a function of time and frequency. The central part of the spectrum is blocked by a notch filter. Shot number 89510.

center, close to the tangent radius of the neutral beam injector. The majority of the beam ions present in the scattering volume are thus ionized with a velocity close to parallel to the static magnetic field. The spatial distribution of ICRH heated fast ions is generally predicted to fall off very rapidly on the high field side of the ICRH resonance layer [38,39]. This suggests that the fast ions in the scattering volume in shot 89510 are mainly beam ions.

Sawteeth are in clear evidence in the ion velocity distribution measured in shot 89510 during the NBI flattop for velocities in the range $0.5\text{--}0.9 \times 10^6$ m/s, but not at higher velocities. This result is reproducible for shots with the measurement on the high field side and velocities resolved in a direction near perpendicular to the magnetic field. In other shots, where either the measurement was on the low field side and near perpendicular velocities resolved or the resolved direction was near parallel to the magnetic field and the measuring volume close to the vessel center, there was no evidence of sawtooth activity in the ion velocity distribution. This despite the presence of sawteeth with the same magnitude and period as in shot 89510.

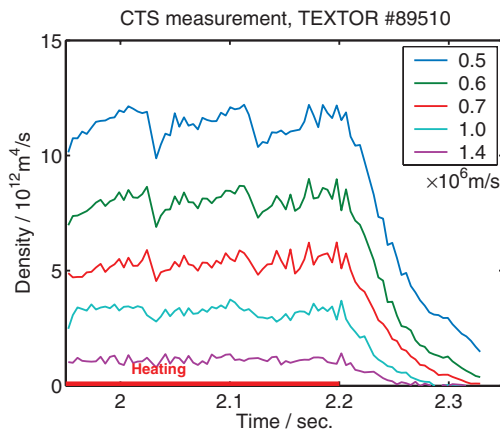


FIG. 5 (color). Ion phase space density vs time at a number of velocities. Auxiliary heating is on until 2.2 seconds. Sawteeth are in evidence at lower velocities but not at higher.

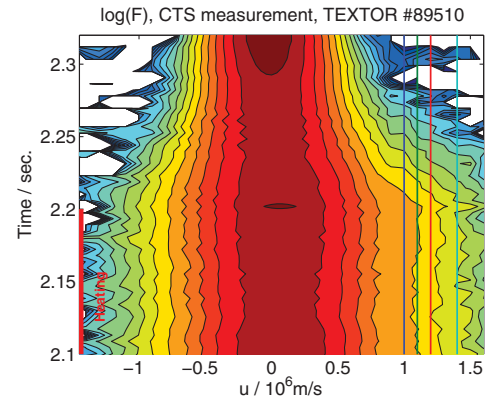


FIG. 6 (color). Contour plot of the logarithm of the measured ion velocity distribution. The auxiliary heating was turned off at $t = 2.2$ s. Time traces are shown in Fig. 8(a) for the velocities indicated in this figure with vertical lines.

The auxiliary heating was turned off at $t = 2.2$ s, after which the fast non-Maxwellian part of the velocity distribution slows down and thermalizes. The measured relaxation of the fast-ion velocity distribution, shown in Figs. 6 and 8(a), is compared with a numerical Fokker-Planck simulation [40] for a homogenous plasma shown in Fig. 7. The Fokker-Planck simulation uses the electron density measured by interferometry and the electron temperature from the ECE and Thomson scattering diagnostics as input. The computed temperature and drift of the bulk ion distribution are the results of interaction with the electrons and the fast ions and of an assumed additional constant loss of energy and momentum intended to represent transport away from the hot center. The latter two are represented by confinement times for ion energy and momentum (200 and 55 ms, respectively), both of which are set for the best fit in the flattop period. Their values are kept constant throughout the modeling including the slowing down period. The beam source rates are best estimates from the NBI data, and the particle confinement time is set to match the measured density. The critical velocity

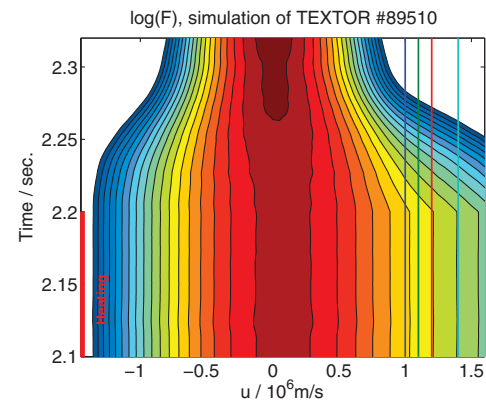


FIG. 7 (color). Contour plot of the logarithm of the simulated distribution function. Time traces are shown in Fig. 8(b) for the velocities indicated in this figure with vertical lines.

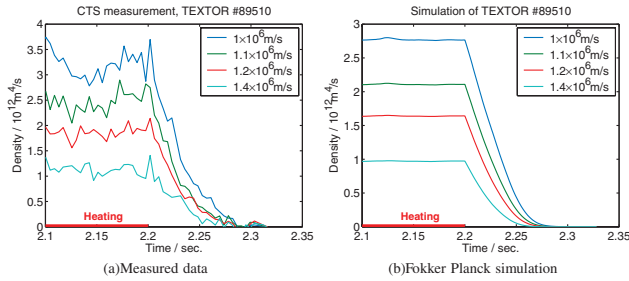


FIG. 8 (color). Time traces of the ion phase space density at a number of velocities. (a) Experimental and (b) model data are compared.

above which fast ions mainly heat electrons is greater than the injection velocity of the beam ions, which is why direct beam heating of bulk ions is accounted for in the modeling. When the heating is turned off, the measured slowing down rates match remarkably well the simulated slowing down rates as may be seen in Figs. 8(a) and 8(b).

In conclusion, we have obtained for the first time measurements of the temporal evolution of fast-ion velocity distributions using collective Thomson scattering. Such measurements are expected to become routine at the TEXTOR tokamak. The evolution of the ion velocity distribution in connection with sawteeth was measured, and notable dependencies on velocity, resolved velocity direction, and spatial location were apparent. The relaxation of the ion velocity distribution after switch off of auxiliary heating could be resolved and agreed remarkably well with Fokker-Planck simulations. These results represent a breakthrough for the use of millimeter-wave collective Thomson scattering for diagnosing confined fast ions in fusion plasmas and are an important milestone in preparing this diagnostic method for use at ITER.

*Electronic address: henrik.bindslev@risoe.dk

- [1] W. W. Heidbrink and G. Sadler, *Nucl. Fusion* **34**, 535 (1994).
- [2] J. Jacquinet *et al.*, *Nucl. Fusion* **39**, 2471 (1999).
- [3] S. D. Pinches *et al.*, *Plasma Phys. Controlled Fusion* **46**, B187 (2004).
- [4] M. N. Rosenbluth and P. H. Rutherford, *Phys. Rev. Lett.* **34**, 1428 (1975).
- [5] C. Cheng and M. Chance, *Phys. Fluids* **29**, 3695 (1986).
- [6] V. S. Belikov, Y. I. Kolesnichenko, and V. V. Lutsenko, *Nucl. Fusion* **35**, 207 (1995).
- [7] W. Kerner, D. Borba, S. Sharapov, B. Breizman, J. Candy, A. Fasoli, L. Appel, R. Heeter, L. Eriksson, and M. Mantsinen, *Nucl. Fusion* **38**, 1315 (1998).
- [8] K. Wong, *Plasma Phys. Controlled Fusion* **41**, R1 (1999).
- [9] D. J. Campbell *et al.*, *Phys. Rev. Lett.* **60**, 2148 (1988).
- [10] J. Graves *et al.*, *Plasma Phys. Controlled Fusion* **47**, B121 (2005).
- [11] Y. Kolesnichenko, V. Lutsenko, R. White, and Y. Yakovenko, *Nucl. Fusion* **40**, 1325 (2000).
- [12] H. Duong and W. Heidbrink, *Nucl. Fusion* **33**, 211 (1993).
- [13] F. B. Marcus, J. M. Adams, D. S. Bond, M. A. Hone, P. J. A. Howarth, O. N. Jarvis, M. J. Loughlin, G. J. Sadler, P. Vanbelle, and N. Watkins, *Nucl. Fusion* **34**, 687 (1994).
- [14] ITER final design report, design requirements, and guidelines level 1 (drg1), Report No. g a0 gdrd 2 01ã07ã13 r 1.0, 2001.
- [15] V. Mukhovatov, R. Bartiromo, D. Boucher, and A. Costley, *Diagnostics for Experimental Thermonuclear Fusion Reactors 2* (Plenum, New York, 1998), Chap. 2, p. 25.
- [16] H. Bindslev, J. A. Hoekzema, J. Egedal, J. A. Fessey, T. P. Hughes, and J. S. Machuzak, *Phys. Rev. Lett.* **83**, 3206 (1999).
- [17] H. Bindslev, F. Meo, and S. B. Korsholm, report, EFDA Contract No. 01.654, 2003.
- [18] H. Bindslev, F. Meo, E. Tsakadze, S. B. Korsholm, and P. Woskov, *Rev. Sci. Instrum.* **75**, 3598 (2004).
- [19] J. Egedal, H. Bindslev, R. Budney, and P. Woskov, *Nucl. Fusion* **45**, 191 (2005).
- [20] A. Sitenko and Y. Kirochkin, *Sov. Phys. Usp.* **9**, 430 (1966).
- [21] R. Aamodt and D. Russel, *Nucl. Fusion* **32**, 745 (1992).
- [22] H. Bindslev, *Plasma Phys. Controlled Fusion* **35**, 1615 (1993).
- [23] H. Bindslev, *J. Atmos. Terr. Phys.* **58**, 983 (1996).
- [24] H. Bindslev (Russian Academy of Sciences, Institute of Applied Physics, Nizhny Novgorod, 1996), Vol. 1, pp. 109–128.
- [25] R. Behn, D. Dicken, J. Hackmann, S. A. Salito, M. R. Siegrist, P. A. Krug, I. Kjelberg, B. Duval, B. Joye, and A. Pochelon, *Phys. Rev. Lett.* **62**, 2833 (1989).
- [26] P. Woskoboinkow, D. R. Cohn, and R. J. Temkin, *Int. J. Infrared Millim. Waves* **4**, 205 (1983).
- [27] E. Suvorov *et al.*, *Plasma Phys. Controlled Fusion* **37**, 1207 (1995).
- [28] J. Hoekzema *et al.*, *Rev. Sci. Instrum.* **68**, 275 (1997).
- [29] J. Machuzak, G. J. Woskov, P. P., N. Bretz, H. Park, and H. Bindslev, *Rev. Sci. Instrum.* **68**, 458 (1997).
- [30] T. Kondoh, S. Lee, D. Hutchinson, and R. Richards, *Rev. Sci. Instrum.* **72**, 1143 (2001).
- [31] U. Tartari *et al.*, *Nucl. Fusion* **46**, 928 (2006).
- [32] H. Bindslev, L. Porte, A. Hoekzema, J. Machuzak, P. Woskov, and D. Van Eester, in *Proceedings of the 26th EPS Conference on Controlled Fusion and Plasma Physics, Maastricht, 1999*, edited by R. Pick (European Physical Society, Paris, 1999), Vol. 23J, pp. 765–768.
- [33] H. Bindslev, L. Porte, A. Hoekzema, J. Machuzak, P. Woskov, D. Van Eester, J. Egedal, J. Fessey, and T. Hughes, *Fusion Eng. Des.* **53**, 105 (2001).
- [34] L. Porte, H. Bindslev, F. Hoekzema, J. Machuzak, P. Woskov, and D. Van Eester, *Rev. Sci. Instrum.* **72**, 1148 (2001).
- [35] S. Michelsen *et al.*, *Rev. Sci. Instrum.* **75**, 3634 (2004).
- [36] S. Korsholm *et al.*, *Rev. Sci. Instrum.* **77**, 10E514 (2006).
- [37] H. Bindslev, *Rev. Sci. Instrum.* **70**, 1093 (1999).
- [38] T. Hellsten, T. Johnson, J. Carlsson, L. Eriksson, J. Hedin, M. Laxaback, and M. Mantsinen, *Nucl. Fusion* **44**, 892 (2004).
- [39] V. Kiptily *et al.*, *Nucl. Fusion* **42**, 999 (2002).
- [40] M. N. Rosenbluth, W. M. Macdonald, and D. L. Judd, *Phys. Rev.* **107**, 1 (1957).